IMAGE RECONSTRUCTION AND RESOLUTION ENHANCEMENT ALGORITHM FOR FMCW MEDICAL ULTRASOUND IMAGING SYSTEMS

Michael Lee
Faculty Advisors: Warren S. Grundfest and Hua Lee
Department of Electrical and Computer Engineering
University of California, Santa Barbara
and
Center for Advanced Surgical and Interventional Technology
University of California, Los Angeles

ABSTRACT

This paper presents an overview of the graduate research program on the design and development of the high-performance image reconstruction and resolution enhancement algorithm for an advanced medical ultrasound imaging system. The data acquisition is conducted with a micro flexible transceiver array, operating in the multi-static stepped-frequency FMCW mode. The objective of this system is to perform high-speed high-resolution image reconstruction for biomedical applications.

INTRODUCTION

Medical ultrasound imaging systems typically feature linear phased arrays with rigid, handheld transducers. Due to the limited contact area of these transducers, a significant portion of the reflected echoes is not detected. A conformal transducer array-based imaging system is developed to accommodate the curved body surfaces to enhance the angular coverage, thereby increasing the information contents of image data acquired. With two-dimensional arrays, it is also potential to provide high-quality 3D imagery while eliminating mechanical scanning. This imaging system may also be suitable for image-guided procedures such as biopsies, which are currently performed with active manual transducer repositioning [1,2]. As many ultrasound imaging systems strive for improved imaging depth as well as resolution, a significant engineering challenge arises. The use of higher frequencies (10-20 MHz) to enhance resolution lowers system signal-to-noise ratio (SNR) due to frequency-dependent attenuation. This limitation has provided one of the motivations for adopting the stepped frequency-modulated continuous wave (FMCW) data-acquisition format for the conformal array system. Its advantages over pulse-echo imaging systems have been widely noted for lower peak power and simpler electronics, and have wider dynamic range and lower noise level [3,4]. Therefore, SNR improvements over conventional techniques may translate to greater

image quality [5,6]. With these attributes, it can be expected that a system featuring a conformal transducer array using FMCW signaling will deliver improved image quality compared to traditional ultrasound systems. The novelty of the system has led to broader exploration of transducer architectures for various imaging applications such as intravascular ultrasound (IVUS) and transurethral ultrasound (TUUS) imaging.

FMCW DATA ACQUISITON

The imaging system operates in a stepped-frequency FMCW format, illuminating a volume of interest with an organized sequence of continuous waves. While the FMCW operating modality differs from pulse-echo systems with regard to the form of the received data, both ultimately provide range estimation for image reconstruction. It has been shown that the stepped-frequency FMCW and pulse-echo modalities are time-frequency counterparts, whose data formats can be interchanged using Fourier transformation and scaling operations [7].

The conformal ultrasound transducer functions multi-statically. During a frequency step within the illumination cycle, one array element transmits a CW while all elements function in receive mode. This repeats as another element assumes the role of the transmitter. Therefore, an M-element transducer array will produce M^2 received complex data sequences. Each of the M^2 received complex data sequences consists of N complex data points, corresponding to the sequence of N coherent signals transmitted during a signaling cycle, stepping through a defined frequency band with frequency increment Δf.

$$f = f_0 + k\,\Delta f, \qquad \text{where } k = 0, 1, 2, \ldots, N\text{-}1. \qquad (1)$$

For each frequency, a transmitted CW signal,

$$e_T(t) = E\,\exp(j2\pi ft), \qquad (2)$$

propagates toward and reflects off a distant target. The returned signal detected at a receiver, $e_r(t)$, is of the same form, except for a change in magnitude due to attenuation and target reflectivity, and a change in phase caused by the delay from the round-trip travel time, τ:

$$e_r(t) = AE\,\exp(j2\pi f(t-\tau)), \qquad (3)$$

where $0 < A < 1$ denotes the reflectivity of the target and $\tau = R_{total}/c = (R_1+R_2)/c$, where R_1 is the range from the transmitter to the target and R_2 is the range from the target to the receiving element, and c is the propagation speed in the medium.

Demodulation of the received signal results in:

$$e(k) = e_r(t)\, e_T^{*}(t) \qquad (4)$$

$$= AE^2 \exp(-j2\pi f_0 \tau) \exp(-j2\pi k\Delta f \tau).$$

Because dependence on the index k is found only in one of the exponential factors of Eq. (4), the factor can be matched to the kernel of the *FFT* in order to reveal its relationship to the time domain [8]:

$$\exp(-j2\pi k\Delta f \tau) = \exp(-j2\pi nk/N). \qquad (5)$$

Variable correspondence gives,

$$n = N\Delta f \tau = B\tau, \qquad (6)$$

where B is the operating bandwidth of the FMCW system, defined as $B = N\Delta f$. So, for a point reflector with an associated τ, the demodulated received signal can be represented as the *FFT* spectrum of a point sequence at $n = (B\tau)$ with a complex magnitude of $AE^2 \exp(-j2\pi f_0 \tau)$:

$$e(k) = FFT\ \{\ AE^2 \exp(-j2\pi f_0 \tau)\ \delta(n - B\tau)\ \}. \qquad (7)$$

Thus, the demodulated received signal for the FMCW system and time-delay profile are a Fourier transform pair. Therefore, the time-delay profile can be obtained by performing an inverse Fourier transform on the received data sequence $e(k)$.

IMAGE RECONSTRUCTION

The functionality and mathematical formulation of the stepped-frequency FMCW data-acquisition format indicates that time-delay profiles are the inverse Fourier transform of the acquired spectral data sequences. Since a spectral data sequence is collected corresponding to a pair of transceiver elements, there is a unique time-delay profile associated with each transceiver pair. Subsequently, the time-delay profiles are scaled by the propagation speed for the conversion to range profiles for the space-time image reconstruction.

Given the coordinates of the transducer elements, space-time image reconstruction is achieved by mapping multi-static range profiles onto a discrete 2D matrix of range bins. From the perspective of a particular element pair, each bin is characterized by a total range distance, $R_{total} = R_1+R_2$. If a point target were to exist at that bin location, R_{total} denotes the range traveled by the acoustic wave from the transmitter, to the target, and then to the receiver. The range profile for that element pair is referenced, and the complex magnitude located at the index R_{total} is added to the bin location of the image matrix. This procedure repeats and information provided by each element pair is superimposed onto the image matrix.

Simulations were performed to test the viability of and further examine the space-time image reconstruction algorithm in the stepped-frequency FMCW environment. Various atypical transducer element configurations, mimicking various possible transducer conformations, and point target distributions were conceptualized on a 2D range bin matrix. Based on the element locations, theoretical range profiles for the targets were generated for each element pair, and then scaled to time-delay profiles according to a human soft tissue propagation speed of 1490 m/s. Each 2048-point time-delay profile was selected to accommodate a maximum delay of 50 μs, setting the sampling frequency at 40.96 MHz.

The mathematical duality between stepped-frequency FMCW data and pulse-echo time-delay profiles permits the theoretical time-delay profiles to be converted to FMCW data through an *FFT* operation. Appropriate frequency components in the spectra were selected to model the desired limited bandwidth of the system. The modified spectra were then converted back to form band-limited time-delay profiles for image formation.

Each reconstructed image shown in Figs. 1 and 2 represents a 3 cm by 3 cm area (with 150 by 150 range bins), with elements depicted in red. The dimension of each range bin was selected to reflect the scale of the range resolution. Fig. 1 shows the simulated reconstruction of a dense group of five point targets, as close as 1.1 mm apart, located near the center of each image. The elliptical patterns from contributing element pairs could be clearly observed. Background artifacts were due to the band-limiting of the time-delay profiles. Their prominence was significantly lessened with larger operating bandwidth, as evident in Fig.(1-a) at 4 MHz bandwidth, and Fig.(1-b) at 1 MHz bandwidth.

Comparing Fig.(1-b) with Fig.(1-c) reveals the effect of aperture size; while both images feature identical target distributions resolved with five elements, high non-target bin values were noticeably fewer and more localized around the targets when imaged with elements spread farther apart. Notably, in the case of the smaller aperture seen in Fig.(1-c), 160 bin values were greater than 40% of its average target bin magnitude, whereas only 75 bin values in Fig.(1-b) were greater than 40% of its average target bin magnitude. These findings underscore the advantage of increased angular coverage supported by large-aperture conformal arrays, resulting in lower target ambiguity.

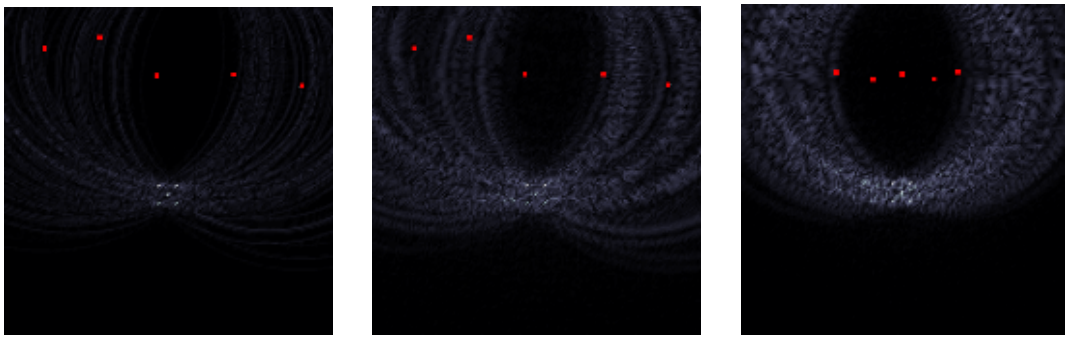

Fig. 1: Five point targets imaged with five irregularly spaced transducer elements. Transceivers are shown in red. (a) 4 MHz (left), (b) 1 MHz (center), (c) 1 MHz (right).

Similarly, full 360-degree element coverage around an identical five-point target distribution, shown in Fig.(2-a), resulted in excellent target clarity with 0.25 MHz bandwidth. Though this arrangement encapsulated the concept of a conformal, inward imaging array, the same reconstruction algorithm can be applied in an outward manner. Fig.(2-b) shows the image of five similar targets resolved with a circular array illuminating radially. The five targets were successfully resolved using an operating bandwidth of 1 MHz.

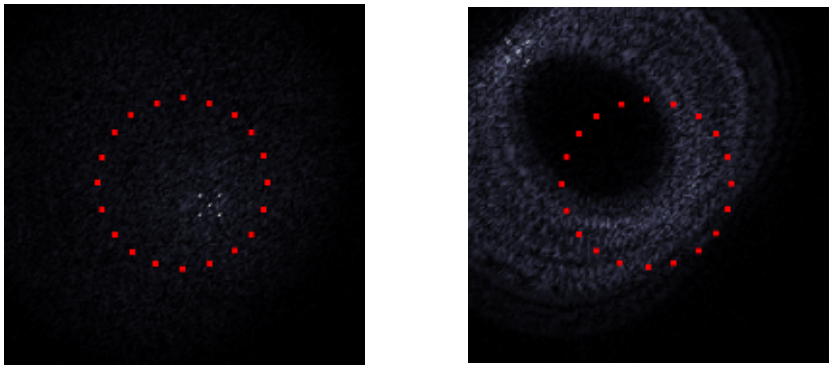

Fig. (2-a): (left image) Inward imaging with 0.25 MHz bandwidth.
Fig. (2-b): (right image) Outward imaging with 1 MHz bandwidth.

RESOLUTION ENHANCEMENT

One important observation is that, at a position *(x, y, z)* in the region of interest, the reconstructed image is the result of the superposition of a collection of backward propagated wave-field vectors in the form of an integral,

$$\hat{s}(x, y, z) = \iiint_R g(x', y', z') h^*(x - x', y - y', z - z') dx' dy' dz' \qquad (8)$$

where ***R*** here denotes the aperture coverage. This implies the value of the final image is in proportion to the mean value of this vector set. Secondly, due to curate phase match and cancellation, at the locations of the point sources, the phase terms are approximately zero, thus the vectors become real and positive scalars, which translates into greater sum with smaller variance. This simple observation indicates that the statistics of the wave-field vectors consistently have large mean value and small variance at the location of the scatters. Otherwise, the statistics give small mean and large variance. Based on this observation, it has been proposed to utilize the variance to improve the resolving capability numerically in the form

$$\hat{s}'(x, y, z) = \frac{m(x, y, z)}{e(x, y, z)} \qquad (9)$$

where $m(x,y,z)$ and $e(x,y,z)$ denote the mean value and enhancement operator of the wave-field vector set at the location (x,y,z) respectively [10]. The enhancement operator can be written in the general form of

$$e(x, y, z) = c + d\, v^p(x, y, z) \qquad (10)$$

where p is the power of the variance image $e(x, y, z)$. The constants c and d are real and positive weighting coefficients for computation stability purpose. The coefficients are selected most effectively according to the noise statistics.

The enhancement operator, $e(x,y,z)$, gives amplification at the scatter locations and attenuation to the background fluctuation where targets are absent. As a result, the operator provides an effective layer of enhancement to the backward propagated images. Fig. (3-a) shows the original image of six scatters in three pairs, and Fig. (3-b) is the enhanced image with first-order variance profile.

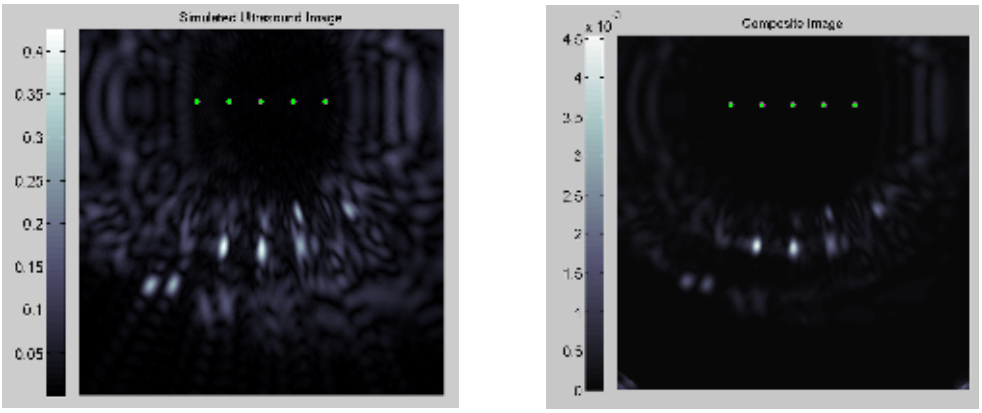

Fig. 3: (a) Original image (left) and (b) enhanced image (right).

As illustrated, the image reconstruction procedure is a two-step process, with first the formation of the range profiles, followed by the backward propagation process mapping the range profiles to the region of interest. The computation of the mean-value image and the variance profile can also be organized into a two-step cascade format, for effective integration with the image formation algorithm.

CONCLUSION

This paper described a space-time image reconstruction and resolution enhancement algorithm for a conformal ultrasound array imaging system, operating in the stepped-frequency FMCW modality. The algorithm was implemented to accommodate the use of irregular array structures, which is crucial to the system design objectives. To document and illustrate the resolving capability and system performance, a complete collection of simulations was conducted for various levels of available spectral bandwidth and aperture sizes. The technical advantages of the FMCW system, including signal processing analysis, image reconstruction, and enhancement algorithm, were illustrated. Although the element configurations were initially implemented for the inward-imaging format of a conformal array system, this paper also demonstrated that the reconstruction algorithm can function effectively in an outward-imaging mode, which can have significant applications in TUUS prostate imaging and IVUS. This work has provided the foundation for the expansion to high-resolution 3D inward and outward imaging algorithms for 2D flexible ultrasound arrays.

ACKNOWLEDGMENT

This research was supported by the Telemedicine and Advanced Technology Research Center (TATRC), Department of Defense under award numbers W81XWH-07-1-0672 and W81XWH-07-1-0668.

REFERENCES

[1] Singh, R.S., Culjat, M.O., Vampola, S.P., Williams, K., Taylor, Z.D., Lee, H., Grundfest, W.S., Brown, E.R., "Simulation, fabrication, and characterization of a novel flexible, conformal ultrasound transducer array," *Proceedings of the 2007 IEEE Ultrasonics Symposium*, pp. 1824-1827, 2007.

[2] Singh, R.S., Natarajan, S., Lee, M., Bennett, D.B., Cox, B.P., Brown, E.R., Grundfest, W.S., Lee, H., Culjat, M.O., "Conformal ultrasound imaging system," *Acoustical Imaging 30*, 2011.

[3] Nicolaescu, I., van Genderen, P., Van Dongen, K. W., van Heijenoort, J., Hakkaart, P., "Stepped frequency continuous wave radar-data preprocessing," *Proceedings of the 2nd International Workshop on Advanced GPR*, pp. 177-182, 2003.

[4] Stove, A.G., "Linear FMCW radar techniques," *IEE Proceedings-F*, 139(5), pp. 343-350, 1992.

[5] O'Donnell, M., "Coded Excitation System for Improving the Penetration of Real-Time Phased-Array Imaging Systems," *IEEE Trans. Ultrason., Ferroelect., Freq. Contr.*, 39(3), pp. 341-351, 1992.

[6] Chiao, R.Y., and Hao, X., "Coded Excitation for Diagnostic Ultrasound: A System Developer's Perspective," *IEEE Trans. Ultrason., Ferroelect., Freq. Contr.*, 52(2), pp. 160-170, 2005.

[7] M. Lee, R.S. Singh, M.O. Culjat, S. Natarajan, B.P. Cox, E.R. Brown, W.S. Grundfest, H. Lee, "Waveform synthesis for the design and image reconstruction of step FMCW ultrasound imaging systems with conformal transducer arrays," *Proceedings of SPIE Medical Imaging 2009: Ultrasonic Imaging and Signal Processing*, 2009.

[8] Lee, H., and Wade, G., "Resolution for Images from Fresnel or Fraunhofer Diffraction using FFT," *IEEE Trans. Sonics and Ultrason.*, 29(2), p. 151, 1982.

[9] Mensa, D.L., *High Resolution Radar Imaging*, Artech House, Dedham, 1981.

[10] Hua Lee and Glen Wade, "Resolution Enhancement on Phase-Only Reconstructions," *IEEE Transactions on Sonics and Ultrasonics*, vol. SU-29, no. 5, pp. 248-250, September 1982.